Rossby waves on the Sun revealed by solar hills

J.R. Kuhn[1] *& J. D. Armstrong*[1] *& R. I. Bush*[2] *& P. Scherrer*[2]

(1) - Institute for Astronomy

University of Hawaii

Honolulu-HI-96822

(2) - Stanford University

Stanford-CA 94305

3/2/00 DRAFT

It is a longstanding puzzle that the Sun's photosphere – its visible 'surface' – rotates differentially with the equatorial regions faster than the poles. Several years ago Plaskett[1], motivated by observations of largescale east-west currents in the Earth's atmosphere, suggested that waves analogous to terrestrial Rossby waves could explain the solar differential rotation. While there is no evidence that the Sun's differential rotation is driven by Rossby waves, modern calculations do confirm that one branch of low-frequency stellar oscillations called r-modes (which are the global solar analog of Rossby waves) has properties which are strongly constrained by the differential rotation[2]. Here we report the detection of a likely

surface manifestation of these global oscillations: 100 m-high hills in the photosphere, spaced uniformly over the Sun's surface. These are particularly interesting, since model calculations[2] have shown that the solar differential rotation (in contrast with uniform rotation) causes large fractional changes in the oscillation frequencies and amplitudes of r-modes. This exquisite sensitivity to the interior rotation makes the detection and observation of r-modes and their properties an excellent probe of the solar interior.

Rossby waves are effectively driven by coriolis forces and are observed in the oceans as large scale (hundreds of kilometers) east or west propagating sea-surface height variations. Satellite measurements[3] show that these 5cm high waves are nearly stationary (with respect to the rotating Earth), requiring tens of years to cross the Pacific. The notion that global Rossby, or inertial, waves could exist within a rotating star was first described in calculations by Papaloizou and Pringle[4]. They named these toroidal oscillations r-modes, after Rossby waves. Unlike the intermediate period g-modes[5], whose properties are determined by bouyancy restoring forces, the nearly incompressible r-modes are subject to coriolis forces and have periods which are near the rotation period. They have not been convincingly observed, but detailed calculations [2,6,7] imply that these modes are a potent probe of the largest structures in the solar convection zone, since they sample both the solar rotation and the large-scale convection timescales. With sufficient amplitude, r-modes will even affect a star's convection and differential rotation flows as suggested in ref. 1.

The Michelson Doppler Imager (MDI) aboard the Solar and Heliospheric Observatory (SoHO) was designed primarily for Doppler observations, although it has produced unique astrometric data because of its accurate pointing and imaging capability from above the Earth's atmosphere. Recently MDI improved on other attempts to measure the static solar limb shape by achieving an uncertainty of less than one milliarcsec[8] in the solar quadrupole and hexadecapole shape. Figure 1 illustrates the astrometric sensitivity of the technique – here the solar shape distortion produced by global p-modes has been detected. These intermediate spherical harmonic degree, 5-min period modes have radial amplitudes of about 15 cm/s[9] so that one oscillation mode produces a limb displacement amplitude of about 10 microarcseconds. This is consistent with the amplitude of the ridge structure displayed in Figure 1 as it was measured from 8 hours of 1 minute cadence MDI solar limb data.

Longer period oscillation measurements are possible using the nearly continuous MDI dataset obtained between April 19, 1996 and June 24, 1998[10]. Analysis of the MDI limb timeseries (figure 2) clearly shows excess low frequency power on all spatial scales below 25 μHz. The corresponding displacement velocity amplitude in mm/s (figure 3) shows an obvious power excess near 20μHz with a root-mean-square velocity amplitude of about 0.3 mm/s. This is not likely to be caused by low radial and angular order solar g-modes because they more efficiently penetrate the convection zone to reach the photosphere at higher frequencies corresponding to periods of one to a few hours[5].

The temporal signature of a photospheric structure (e.g. a standing wave pattern) as it traverses the limb due to the solar rotation can be detected in the temporal power spectrum of the limb displacement computed as a function of position angle (or solar latitude). The apparent sawtooth-shaped power enhancement in Figure 4 is consistent with a corotating photospheric modulation having a latitude-independent transverse scale of $8.7 \pm 0.6 \times 10^4$km. As expected for a solar (versus an instrumental) phenomenon, the power distribution near the poles is noticeably smeared by the 7 degree inclination of the solar rotation axis from the normal direction to the ecliptic plane. We also analyzed data from approximately one month when MDI was rotated several degrees from its nominal roll angle. Data obtained during this period confirms that this signal is not associated with the MDI instrument, since the "sawtooth" power distribution, calculated as in Fig. 4, rotated in apparent position angle by an amount in agreement with the new MDI roll angle.

This regular structure of 100m high photospheric "hills", uniformly spaced over the surface of the Sun with a characteristic separation of approximately

90,000km, is most plausibly explained as the corotating photospheric signature of long period r-modes. It is not surprising that these modes have been invisible from the ground, since long period oscillations are more readily detected from astrometric (shape) measurements from space than from even the most sensitive groundbased Doppler observations. At low frequencies solar Doppler data are dominated by incoherent velocity noise from the convection zone. At low temporal frequencies even a small velocity amplitude oscillation may be extracted from the convective noise in limb shape measurements because the limb displacement amplitude grows linearly with oscillation period (for a constant velocity amplitude), while the convection noise contributes only incoherently.

Could this signal be produced by the solar supergranulation[11]? With a transverse scale of 30,000 km, the timescale for limb perturbations due to these features would be 4 hours, or about one third of the period of the observed 20μHz power excess. We could hypothesise that only the largest supergranule elements are detected at the limb because of foreshortening and projection effects. Then, depending on the statistical distribution of supergranules, we might find only one-in-two or one-in-three of them to be visible at the limb. With the assumption that supergranulation is a random convection process we expect the timeseries of limb perturbations to be random, but with a mean time between limb perturbations of, say, 11 hr. This stochastic timeseries (called a "random telegraph signal"[12]) has a well known power spectrum in the form of a Lorentzian, $P(\omega) = \frac{P_0}{1+(\omega/\omega_0)^2}$. Thus, the existence of a mean timescale (11 hr in this case) leads to a spectrum which is monotonic, and which shows a $1/\omega^2$ decline beyond the characteristic frequency. Only if there is long range coherence in the timeseries (over many characteristic timescales) will the power spectrum yield a *peak* at the average temporal frequency. Thus, a test of the stochastic or supergranule hypothesis requires looking for a Lorentzian form to the low frequency spectrum.

The spectrum from a single latitude bin is too noisy to distinguish a monotonic excess power signal (a Lorentzian) from the generally increasing displacement noise power toward lower frequencies. Combining spectra from a range of latitude bins improves the signal-to-noise ratio. We find a Gaussian peak in the mean spectrum (Fig. 5) with a center frequency of 18μHz. The existence of a spectral peak suggests that at least a portion of the low frequency power is not caused by supergranules. Although the spectrum also contains a displacement "background" signal which increases to lower frequencies, the peak signal (corresponding to a 15hr period) is best described as a low-Q oscillator. It has long range order and is *not* a stochastic "random telegraph." A standing wave is a natural mechanism for producing such a lattice of solar "hills". Wolff[13,14] previously suggested that a largescale photospheric nodal pattern generated by phaselocked r-modes would evolve over timescales of a few days – a result in qualitative agreement with the low-Q oscillator we see here in the mean limb displacement power spectrum. If r-modes are driven by the largest scales of convection we should also expect a characteristic lengthscale on the order of the 2×10^5km depth of the convection zone. The transverse scale we observe is a factor of two smaller but is plausibly consistent.

The magnitude of the vertical displacement is also energetically reasonable. If subphotospheric convection is spatially organized by these Rossby modes then even velocities of 100m/s (a small fraction of measured photospheric convective velocities) are energetic enough to uplift the overlying photosphere by the observed 100m vertical height. While it remains to be seen from detailed model calculations exactly how global solar r-modes could be excited, the existence of a corrugated photosphere with long range order is good evidence for these oscillations.

Address correspondence or request for materials to jkuhn@solar.stanford.edu.

References

1. Plaskett, H.H. The polar rotation of the Sun. *Mon. Not. R. Astron. Soc.* **131**, 407-433 (1966).

2. Wolff, C.L. Linear r-mode oscillations in a differentially rotating star *Astrophys. J.* **502**, 961-967 (1998).

3. Chelton, D.B. and Schlax, M.G. Global observations of oceanic Rossby waves. *Science* **272**, 234-238 (1996).

4. Papaloizou, J., and Pringle, J.E. Non-radial oscillations of rotating stars and their relevance to the short-period oscillations of cataclysmic variables. *Mon. Not. R. Astron. Soc.* **182**, 423-442 (1978).

5. Kumar, P., Quataert, E., Bahcall, J. Observational searches for solar g-modes: some theoretical considerations. *Astrophys. J.* **458**, L83-85 (1996).

6. Provost, J. Berthomeiu, G., Rocca, A. Low frequency oscillations of a slowly rotation star - quasi toroidal modes *Astron. Astrophys.* **94**, 126-133 (1981).

7. Wolff, C. L. and Blizard, J.B. Properties of r-modes in the Sun *Sol. Phys.* **105**, 1-15 (1986).

8. Kuhn, J.R., Bush, R., Scheick, X., and Scherrer, P. The Sun's shape and brightness. *Nature* **392**, 155-157 (1998).

9. Lazrek, M. et al. First results on p-modes from GOLF experiment. *Sol. Phys.* **175**, 227-246 (1997).

10. Scherrer, P.H., et al. The Solar Oscillations Investigation – Michelson

Doppler Imager *Sol. Phys.* **162**, 129-188 (1995).

11. Schrijver, C.J., Hagenaar, H. J., Title, A. M. On the Patterns of the Solar Granulation and Supergranulation *Astrophys. J.* **475**, 328-337 (1997).

12. Rice, S.O. Mathematical Analysis of Random Noise. *Bell Systems Tech. Jour.* **23**, 1-162 (1944).

13. Wolff, C.L. Distinctive patterns on the surface of slowly rotating stars whose oscillations are non-linearly coupled. *Astrophys. J.* **193**, 721-727 (1974).

14. Wolff, C. Oscillation convection coupling: cause of supergranulation. *Astrophys. J.* **443**, 423-433 (1995).

We wish to thank Julia Saba, Craig DeForest and Joseph Covington for their assistance in operating the MDI instrument during these observations. We are particularly grateful to Rick Bogart and to Xania Scheick for their help with the limb software analysis effort.

Figure Captions

Figure 1: This figure shows the two-dimensional power spectrum of the limb displacement. This was derived from an 8 hour period of 1 min cadence data obtained in 0.7 degree wide position angle bins. The horizontal axis corresponds to the angular frequency while the vertical axis plots the temporal frequency. We note that a measurement at angular frequency k tends to sample spherical harmonic modes of angular and azimuthal order equal to k ($l = m = k$). The image greyscale indicates the logarithm of the derived limb displacement power in units of arcsecond^2. This shows the complete spectrum including Nyquist aliasing about the central temporal and spatial frequencies. The p-mode ridge structure near 3mHz frequencies is clearly observed here in the changing solar limb shape.

Figure 2: This figure shows the two-dimensional, low frequency, power spectrum of the MDI limb timeseries. During 26 months a 6 pixel wide annulus which includes the solar limb was generated every 12 minutes[9]. These data were analyzed as described in ref. 7 to reveal the limb position and brightness in 512 position angle bins covering the solar limb, and with 98304 temporal samples at a cadence of 12min. Gaps from telemetry problems and instrument mode changes corrupted about 3% of this timeseries. Measurements obtained after the SOHO disruption on June 25, 1998 and after the spacecraft reacquired the Sun on Sept. 16, 1998 were also not included here because of a

higher noise background caused by frequent spacecraft and experiment operating mode changes. The horizontal axis describes the angular frequency as obtained from the discrete transform with respect to the limb position angle. Slowly varying instrumental noise was minimized by removing a 180 degree wide boxcar average from each limb data record. An 8.3 day boxcar temporal average was also removed to yield a record of the residual temporal fluctuations in the solar limb over a 2.2 year period. The two dimensional fourier transform yields the limb displacement power spectral density in units of arcsec^2 per frequency bin which is displayed here on a logarithmic greyscale.

Figure 3: The root-mean-square limb shape velocity amplitude is plotted here versus frequency. The average displacement power between angular frequencies of 20-256 has been converted to an rms velocity by scaling the amplitude by the temporal frequency. This is plotted on a logarithmic scale here to reveal the mean effective velocity background from 800 days of astrometric observations. The excess power appears here as a bump at a frequency near 20 μHz with a total rms amplitude of 0.3 mm/s.

Figure 4: The power distribution plotted here shows the average power per temporal frequency bin versus position angle. The greyscale describes the average power in units of arcsec^2 per bin on a logrithmic intensity scale. The limb displacement was computed from the residual of a 256 bin running mean of each limb position record. Temporal residuals were then evaluated from

the difference between this computed limb position and an 8.3 day running mean of the 7.1×10^7s duration timeseries. Position angle 0 corresponds to the west limb with increasing angles approaching the north pole. The power spectrum has been smoothed with an 88 point running boxcar average before plotting. The solid line shows the expected frequency of an 8.75×10^4km transverse scale vertical photospheric modulation which is rotating at the photospheric differential rotation rate.

Figure 5: The mean power spectrum averaged over latitude is displayed here. This is computed by assuming the limb power spectra are due to a photospheric displacement pattern, rotating across the limb at various velocities corresponding to the local latitudinal rotation speed. The mean spectrum is obtained by first stretching the frequency scale of each latitudinal spectrum to match the equatorial spectrum (by linear interpolation onto the new frequency domain), and then averaging these on the common frequency domain. A simple shift of each spectrum by a frequency equal to the sawtooth variation with latitude (from fig. 4) also matches the broad power excess at each latitude to the equatorial rate, yielding a mean spectrum which is essentially the same as the scaled frequency result displayed here. The solid line shows a least-squares fit to a gaussian and a power law background distribution. The resulting center frequency is 18μHz.

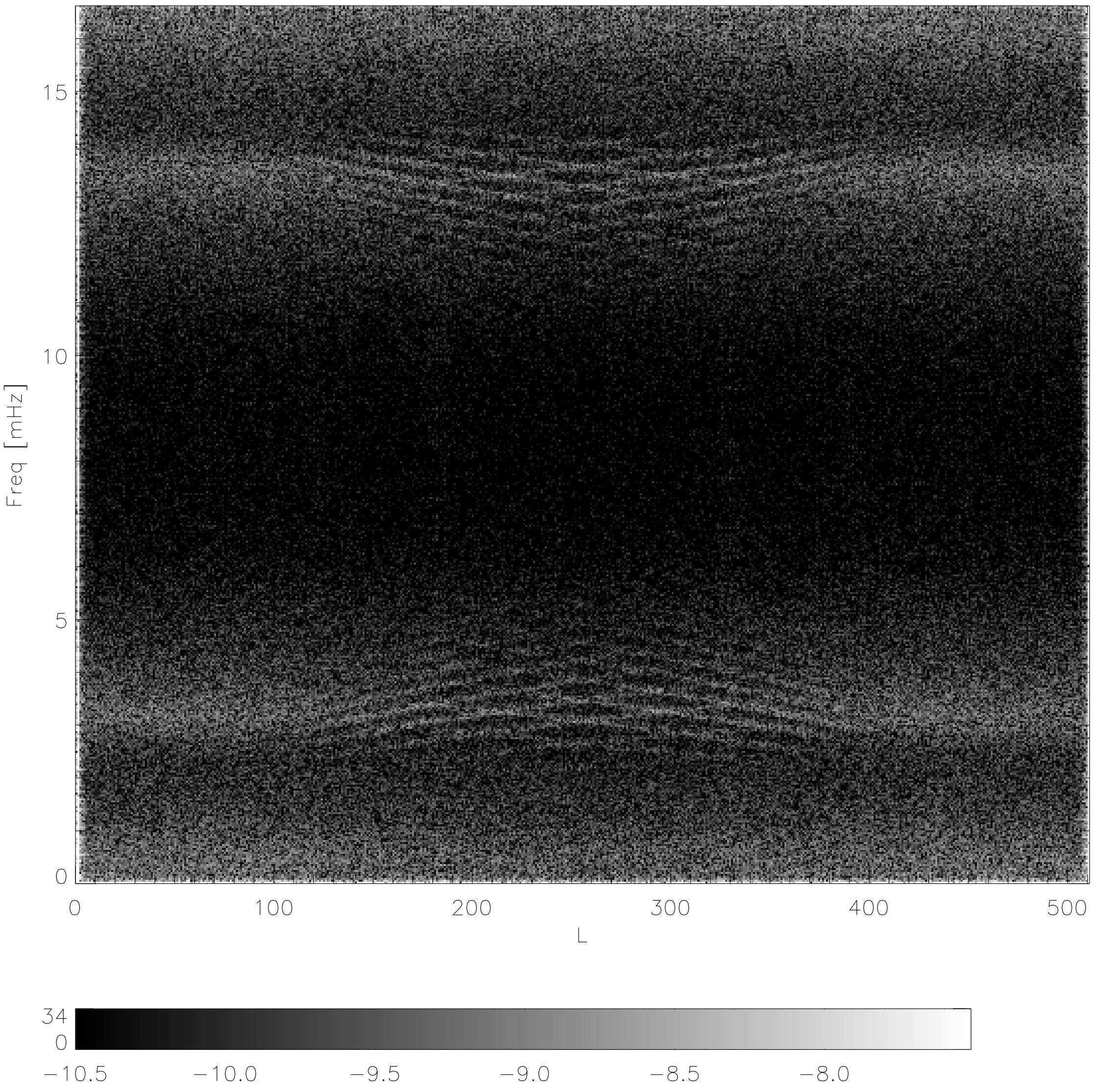
Freq [mHz]
0
5
10
15
L
0
100
200
300
400
500
34
0
−10.5
−10.0
−9.5
−9.0
−8.5
−8.0

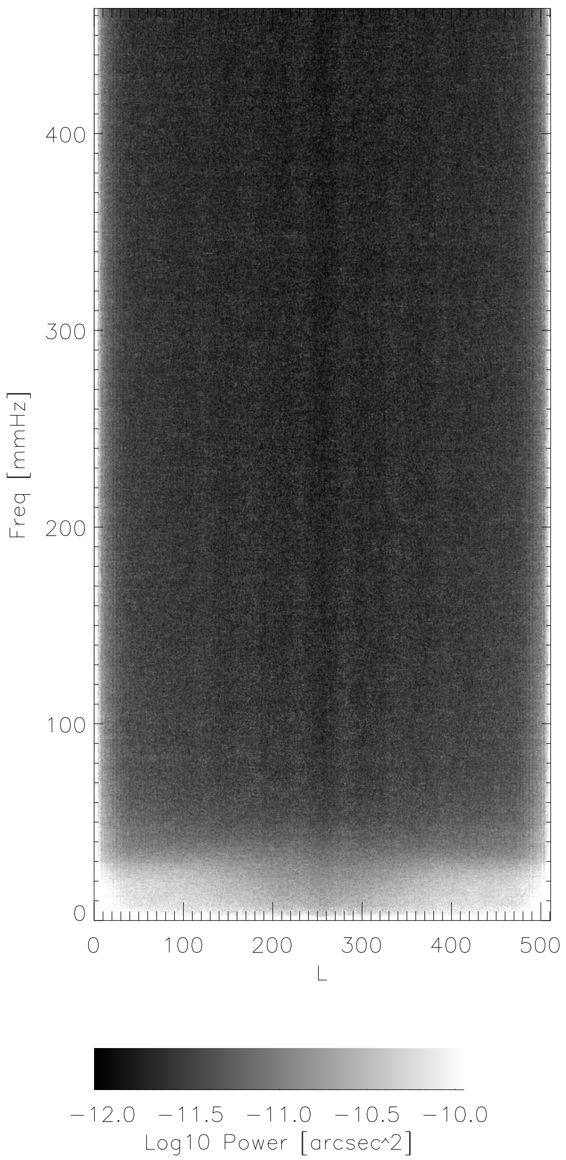

Freq [mmHz]
0
100
200
300
400
L
0
100
200
300
400
500
−12.0
−11.5
−11.0
−10.5
−10.0
Log10 Power [arcsec^2]

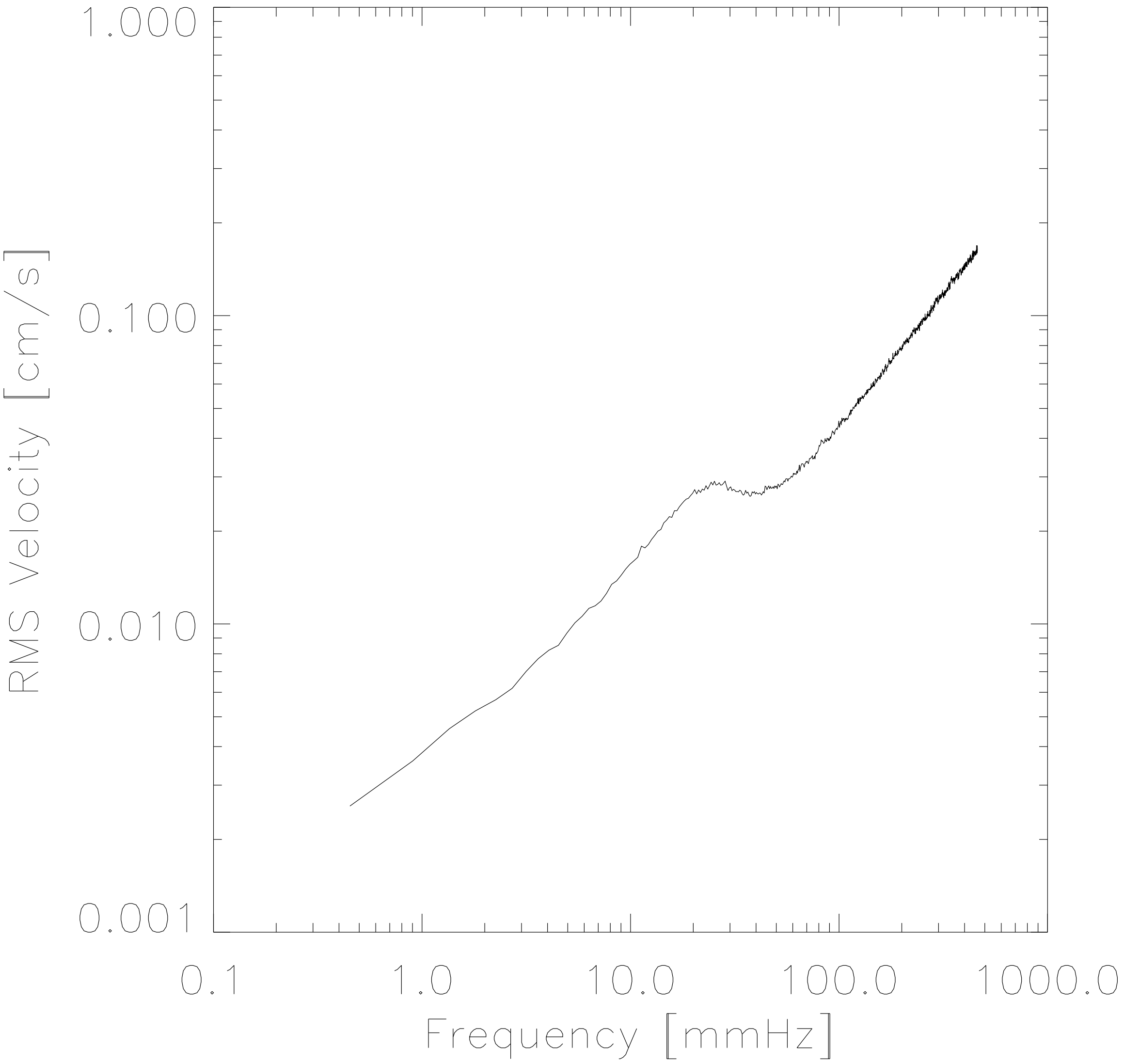
1.000
0.100
0.010
0.001
RMS Velocity [cm/s]
0.1
1.0
10.0
100.0
1000.0
Frequency [mmHz]

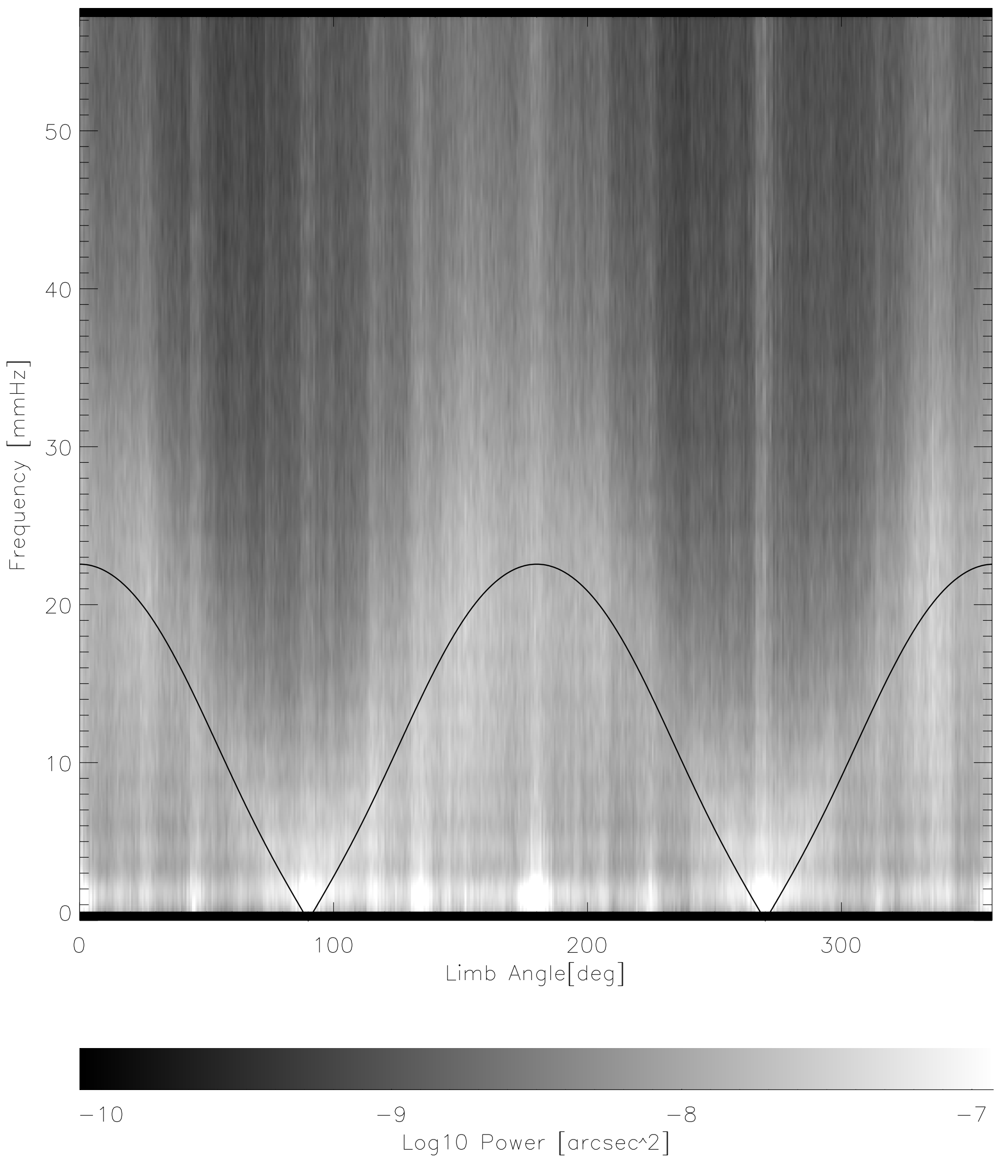
Frequency [mmHz]
0
10
20
30
40
50
0
100
200
300
Limb Angle[deg]
−10
−9
−8
−7
Log10 Power [arcsec^2]

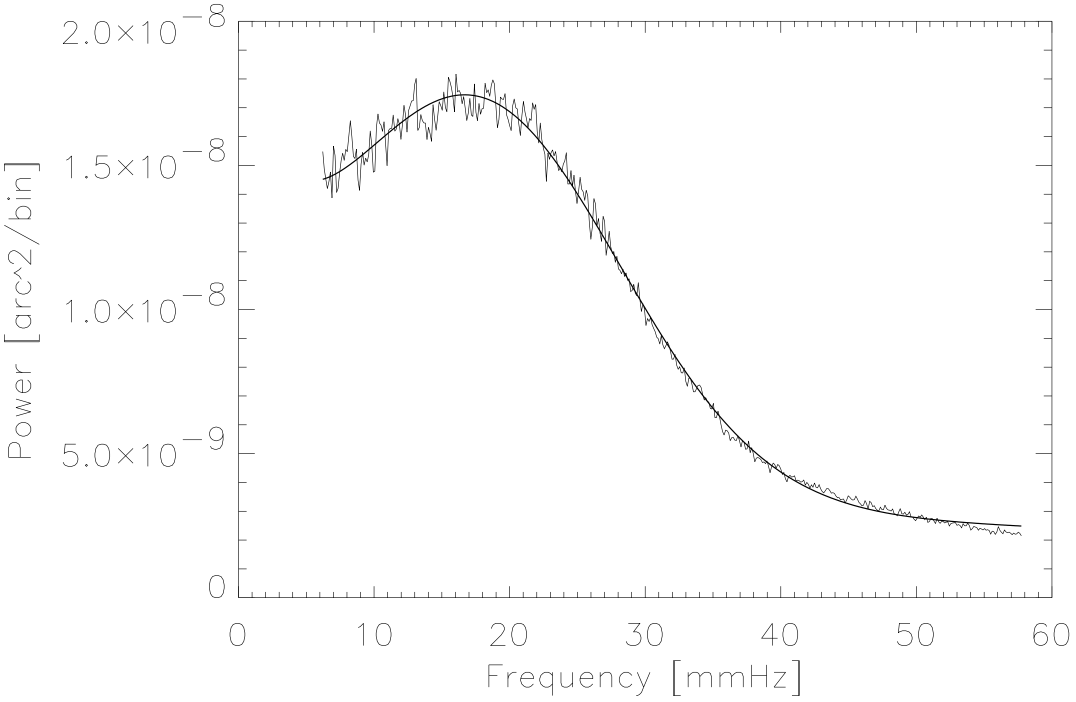
2.0×10⁻⁸
1.5×10⁻⁸
1.0×10⁻⁸
5.0×10⁻⁹
0
Power [arc^2/bin]
0
10
20
30
40
50
60
Frequency [mmHz]